Review article

Technological characterization of kaolin: Study of the case of the Borborema–Seridó region (Brazil)

Fernanda Arruda Nogueira Gomes Silva[a], [✉], [✉], Adão B. Luz[b], João Alves Sampaio[b], Luiz Carlos Bertolino[c], Rosa Bernstein Scorzelli[d], Mathieu Duttine[d] and Flávio Teixeira da Silva[a]

[a]Universidade Federal do Rio de Janeiro (UFRJ), Departamento de Engenharia Metalúrgica e de Materiais (PEMM), Coordenação de Pesquisa e Pós Graduação em Engenharia (COPPE/UFRJ), Avenida Horácio Macedo s/n, bloco F, Ilha da Cidade Universitária, Rio de Janeiro/RJ. Cep. 21941-914, Brasil

[b]Centro de Tecnologia Mineral (CETEM), Ministério da Ciência e Tecnologia (MCT), Avenida Pedro Calmon, 900, Ilha da Cidade Universitária, Rio de Janeiro/RJ. Cep. 21941-908, Brasil

[c]Universidade do Estado do Rio de Janeiro (UERJ), Faculdade de Formação de Professores (FFP), Departamento de Geografia, Rua Francisco Portela, 794, Patronato, São Gonçalo/RJ. Cep. 24435-005, Brasil

[d]Centro Brasileiro de Pesquisas Físicas (CBPF), Ministério da Ciência e Tecnologia (MCT), Rua Doutor Xavier Sigaoud, 150, Urca, Rio de Janeiro/RJ. Cep. 22290-180, Brasil

Abstract

The technological characterization of kaolin from the Borborema–Seridó region has shown that it is predominantly kaolinitic, pseudoplastic and thixotropic; approximately 50% of its particles size is less than 2 μm. By using electronic paramagnetic resonance (EPR) and Mössbauer spectroscopy (ME), it was observed that Fe^{2+} and Fe^{3+} substitute Al^{3+} in octahedral sites of kaolinite. After magnetic separation followed by chemical bleaching, kaolin reached a brightness index of 87.72% ISO and an opacity index of 85.58% ISO, indicating that it can be used mainly as a filler and a coating in the paper industry, paint and pottery, among other industries.

Article Outline

1. Introduction

The pegmatitic province in the region of Borborema–Seridó is located in the northeast of Brazil (Paraíba and Rio Grande do Norte States). In the Junco–Equador region, there are several deposits of kaolin associated with altered pegmatites; in those pegmatites, kaolin is associated with muscovite and quartz (Silva and Dantas, 1997). When compared with the kaolin from the southeast, this kaolin presents much finer well crystallized particles with hexagonal morphology (Wilson et al., 1998).

The most important use of kaolin is in the paper industry and it is estimated that the world's kaolin production is 25 million tons, from which around 10 million are destined to the paper industry as a filler and a coating (Murray and Kogel, 2005). As a coating agent, kaolin requires an adequate combination of brightness and opacity (Luz et al., 2005).

As kaolin brightness is not very high, paper industries normally adopt a blending of kaolin with precipitated calcium carbonate in the place of titanium dioxide, which has higher brightness and opacity but a higher cost. Moreover, this blending may result in a higher processing cost due to the difficulty in pulp dispersion caused by the differences in its zeta potentials and the lower stability of calcium carbonate in acid media.

As a coating agent, kaolin promotes a smooth topography with improved properties to receive ink (Ciullo, 2004) and very fine kaolin particles constitute an interesting color pigment for ultra lightweight coating paper applications (Conceição et al., 2005). The main characteristics of kaolin used as a coating agent are illustrated in Table 1. As a filler, kaolin can be used in a certain amount in order to reduce the amount of celluloses pulp as well as to promote a considerable improvement in the opacity and printability.

Table 1.

Characteristics of kaolin used as a coating agent in the paper industry (Ciullo, 2004).

Characteristics	Descriptions
Particle size	70–90% < 2 μm
Viscosity	≤ 1000 mPa s at 70% of solids
Specific surface area	6–22 m^2/g
Density	2.6
Refraction index	Close to 1.5
Brightness	80–90% ISO

2. Materials and methods

Kaolinite from the Equador Formation and from the micaschists of the Borborema–Seridó region originates from potassic feldspars alterations. Table 2 shows the chemical composition of raw kaolin.

Table 2.

Chemical analysis of the raw kaolin (wt.%).

Oxides	Weight %
SiO_2	67.25
Al_2O_3	23.21
Fe_2O_3	0.60
TiO_2	< 0.01
CaO	0.02
MgO	0.05
Na_2O	0.52
K_2O	0.70
Loss on ignition	8.23

Fig. 1 shows the block diagram used in the beneficiation and characterization of kaolin. After wet sieving, the − 37 μm fraction was selected for the physical and physicochemical concentration steps. The first one was magnetic concentration through high intensity wet magnetic separation in *Boxmag Rapid* equipment, aiming the removal of iron minerals (mainly hematite, goethite and magnetite). In order to achieve an efficient magnetic separation, an agitated pulp with 20% solid was slowly added to the separator. The field intensity was approximately 1400 mT. Due to the small particle size of kaolin, steel wool was used to increase the magnetic field intensity. Despite the low brightness from the non magnetic fraction, the removal of iron oxides at this stage resulted in a substantial economy of chemical reagents during the bleaching step (Domenico, 2000).

[Full-size image](#) (24K)

Fig. 1. Block diagram used in the beneficiation and characterization studies of kaolin from the Borborema–Seridó (Brazil) region.

After magnetic separation, only the non magnetic fraction of kaolin was selected for chemical bleaching studies in oxidant or reducing media. In oxidant conditions, the main aim was to remove organic matter and in reducing conditions to remove iron oxides or hydroxides. In this case, it was important to evaluate if iron oxide/hydroxide was free or associated with muscovite, or as iron ions (Fe^{2+} or Fe^{3+}) in the crystalline structure of kaolinite (Luz and Chaves, 2000).

The kaolin sample was characterized by particle size distribution through *Micromeritics Sedigraph* 5100, optical properties through *Color Touch spectrometer* ISO *Technidyne Corporation* and viscosity measurements through Rheo *Stress* (RS1). Apparent *viscosity* curves were plotted as a function of shear rate for 30% solid content pulps at 25 °C.

In order to identify the mineralogy of kaolin samples and the distribution of iron ions in the crystalline structure of kaolinite several techniques were used: X-ray diffraction (XRD) (*Bruker AXS D5005*) with Co Kα radiation at 35 kV and 40 mA, infrared spectroscopy (IV), *Bomem Hartmann & Braun*, with registrations from 4000 to 400 cm^{-1} and measurements to every 4 cm^{-1}, electronic paramagnetic resonance (EPR) *Brüker* model *ESP300E* spectrometer with spectra recorded at 9.75 GHz (X-band) at room temperature (303 K) and Mössbauer spectroscopy (MS) at room temperature with a source of ^{57}Co.

3. Results and discussion

The particle size distribution of the non magnetic fraction (− 37 μm), Fig. 2, has shown that approximately 48% of kaolin particles were less than 2 μm. It is worth pointing out that the kaolin particle size used commercially in the paper industry is less than 2 μm. Prasad et al. (1991) have shown that a brilliant surface finishing is produced if fine kaolin is used as a coating agent. As a filler, the amount of kaolin is limited; an excess addition of kaolin may decrease the mechanical strength of paper due to the interaction between kaolin and cellulose fibers (Luz et al., 2005).
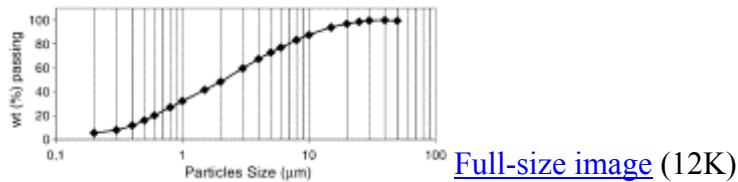
Full-size image (12K)

Fig. 2. Particles size distribution of the − 37 μm fraction, obtained with *Sedigraph* equipment.

The X-ray diffractograms of kaolin − 37 μm and magnetic separation fractions are illustrated in Fig. 3. It was observed that kaolin (− 37 μm) was essentially kaolinitic, with some muscovite and quartz as the main impurities. After high intensity wet magnetic separation, muscovite with some iron oxide was concentrated in the magnetic fraction and kaolinite in the non magnetic fraction. The removal of muscovite from the kaolin feed promoted a reduction of 15% in iron oxide content in the non magnetic fraction, as shown in Table 3.
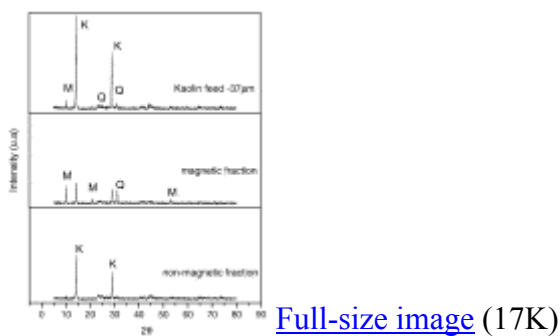

Full-size image (17K)

Fig. 3. X-ray diffraction of − 37 μm kaolin feed, as well as the magnetic and non-magnetic fractions from the high intensity wet magnetic separation. ($V = 35$ kV, $I = 40$ mA, λ KαCo). K — kaolinite, M — muscovite, Q — quartz.

Table 3.

Chemical composition of the − 37 μm kaolin feed and of the non-magnetic fraction.

Oxides	− 37 μm kaolin feed (%)	− 37 μm non-magnetic (%)
Fe_2O_3[a]	0.26	0.22
SiO_2	51.60	45.9
Al_2O_3	36.32	39.2

[a] Percentage of iron converted to Fe_2O_3.
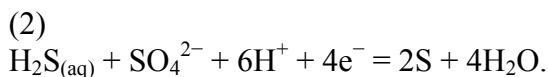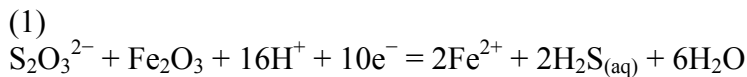
Infrared spectroscopy was used to characterize the − 37 μm kaolin feed and − 37 μm non magnetic fraction, as shown in Fig. 4. The kaolin feed − 37 μm and the non magnetic fraction present similar bands in the region from 300 to 2500 cm^{-1}, which correspond to kaolinite and muscovite bands. In the region near 3600 cm^{-1}, bands 3615, 3652 and 3663 cm^{-1} bands correspond to Al–O–H vibration, which can belong either to kaolinite or muscovite (Marel and Beutelspacher, 1976). The region between 420 and 1170 cm^{-1} presents vibrations Si–O that can belong either to quartz, kaolinite or muscovite. A small inflection in the region of 930 cm^{-1} corresponds to the deformation vibration of the Al–OH–Fe bonds. This kind of bond indicates the substitution of Al^{3+} ions by Fe^{2+} in the crystalline structure of kaolinite.
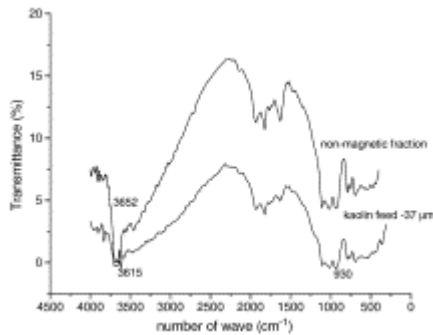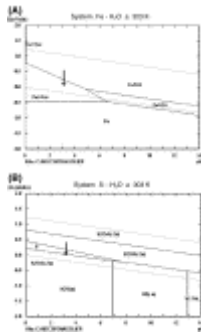
Full-size image (18K)

Fig. 4. Infrared spectra of kaolin feed − 37 μm and of non-magnetic fraction.

The − 37 μm non magnetic fraction was submitted to chemical bleaching in sulfuric acid solution with the addition of a reducing agent (Na$_2$S$_2$O$_4$). Fig. 5 shows the Eh–pH diagrams of Fe-H$_2$O and S-H$_2$O at 298 K, for [Fe] = 10^{-3} mol/L and for [S] = 10^{-3} mol/L. It can be seen that in low pH and in reducing conditions, there is a superposition of the Fe^{2+} and elementary S stability fields, indicating conditions for iron removal (reaction 1) and some feasibility for sulfur precipitation (reaction 2).

(1)
$$S_2O_3^{2-} + Fe_2O_3 + 16H^+ + 10e^- = 2Fe^{2+} + 2H_2S_{(aq)} + 6H_2O$$

(2)
$$H_2S_{(aq)} + SO_4^{2-} + 6H^+ + 4e^- = 2S + 4H_2O.$$

[Full-size image](#) (39K)

Fig. 5. Eh–pH diagram of the Fe-H_2O and S-H_2O systems at 303 K. In (A), iron species, in (B), sulfur species (HSC Chemistry for Windows, 3.0).

Fig. 6 illustrates brightness increase with conditioning time varying the solution pH and keeping constant the $Na_2S_2O_4$ concentration 4.0 kg/t. In this pH range, the bleaching rate was not affected. Otherwise it was observed a slight increase in brightness at lower pH.
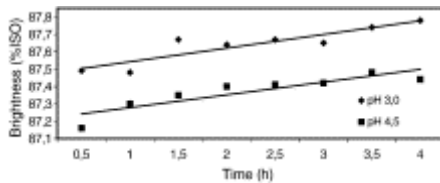
[Full-size image](#) (12K)

Fig. 6. Influence on conditioning time and pH on kaolin brightness index. $[Na_2S_2O_4] = 4.0$ kg/t.

The influence on $Na_2S_2O_4$ concentration was evaluated at pH 3.0, varying the conditioning time, as it can be seen in Fig. 7. Some fluctuation in brightness was observed, but the highest brightness index was for $[Na_2S_2O_4] = 2.75$ kg/t, and 2 h bleaching time. It is expected that at higher concentrations the precipitation of elementary sulfur would be more feasible. It is important to point out that stirring during chemical bleaching should not be very aggressive since the reducing agent oxidates in the presence of air.
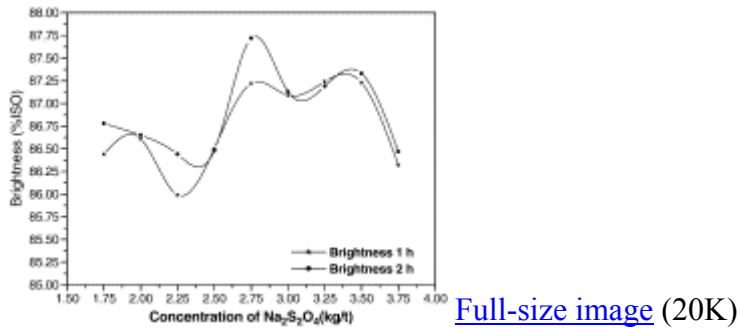
Full-size image (20K)

Fig. 7. Influence on the $Na_2S_2O_4$ concentration and the conditioning time in the kaolin brightness index (pH = 3.0).

As iron removal from the non magnetic fraction after chemical bleaching was only 28 wt.%, this result indicated that iron was also in the crystalline structure of kaolinite. In order to identify and quantify the iron ions in kaolinite, EPR and MS techniques were carried out.

Fig. 8 shows EPR spectrum of a bleached sample. In the region $G \approx 4.0$, it can be seen as two superimposed signals with different degrees of distortion attributed to Fe^{3+} substituting Al^{3+} in the kaolinite crystalline structure (Brindley et al., 1986). The inexistence of a bend region of the non magnetic bleached kaolin between 2000 and 3000 mT (Fig. 8) indicated that iron oxides were completely removed during chemical bleaching.
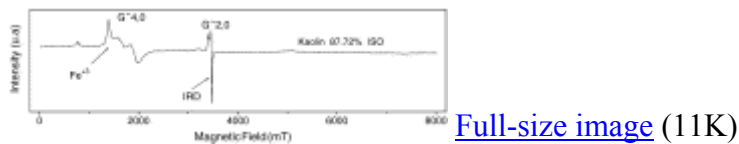

Full-size image (11K)

Fig. 8. EPR spectrum of the chemical bleached kaolin (87.72% ISO). RID (radiation-induced defect).

Fig. 9 shows the EPR spectra of the − 37 μm kaolin feed and of the non magnetic fractions. It can be seen that in both cases there is a bend region between 2000 and 3000 mT mainly in the kaolin feed, which is related to iron oxides associated with muscovite and kaolinite. The signal observed in region of $G \approx 2.0$ is associated with the Radiation Induced Defect (RID) (Clozel et al., 1994).
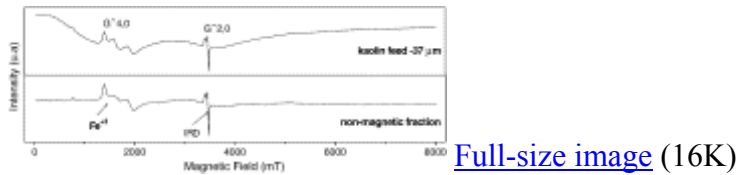
Fig. 9. EPR spectrum of the kaolin feed − 37 μm and of the non-magnetic fraction.

The next step was to identify the distribution of iron ions in the crystalline structure of kaolinite by Mössbauer spectroscopy. Fig. 10 shows Mössbauer spectrum of the bleached kaolin (87.72% ISO) and the Table 4 its hyperfine parameters.
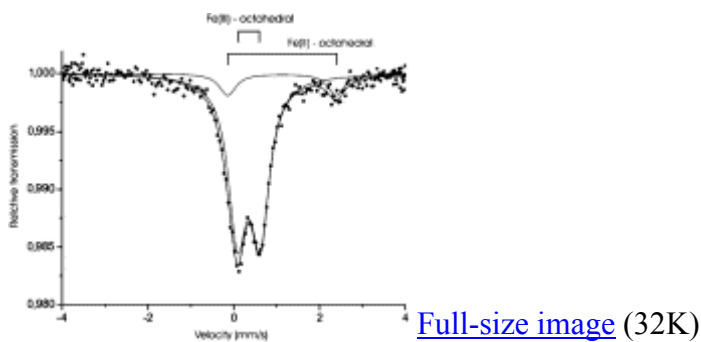
Fig. 10. Room temperature ^{57}Fe Mössbauer spectrum of bleached kaolin (87.72% ISO).

Table 4.

Hyperfine parameters of Mössbauer spectrum of the bleached fraction.

IS (mm/s)	EQ (mm/s)	A (%)	Species
0.35	0.53	88.30	Fe^{3+} octahedral site
1.13	2.53	11.70	Fe^{2+} octahedral site

Rheology and opacity are other important properties for its use in the paper industry. As shown in Fig. 11, the rheological regime of kaolin pulp was characterized as pseudoplastic thixotropic, with a thixotropy value of 112.75/mPa.s. These results are in agreement with the previous data (Conceição et al., 2005).
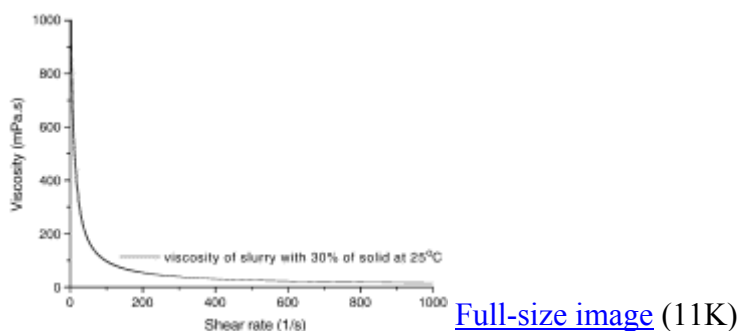
(11K)

Fig. 11. Variation in kaolin's slurry viscosity according to shearing index.

One of the main functions of kaolin in the paper industry is to limit the transmitted light, that is, the higher the refraction index the higher its opacity. Table 5 illustrates the influence on chemical bleaching on the kaolin opacity index (ISO). It was observed that chemical bleaching has practically no influence on kaolin opacity.

Table 5.

Influence on chemical bleaching on kaolin opacity.

Kaolin	Opacity (% ISO)
Fraction − 37 μm	85.38
Bleached (87.72% ISO)	85.98

4. Conclusions

Kaolin from the Borborema–Seridó region is of primary origin, essentially kaolinitic, and associated with quartz, feldspars and muscovite. The − 37 μm fraction corresponds to 47% of the feeding mass. Their main impurities are iron oxide, and Fe^{2+} and Fe^{3+} ions present in the crystalline structure of kaolinite.

The high intensity of wet magnetic separation followed by chemical bleaching removes approximately 0.5% of the iron content in the − 37 μm fraction. This percentage indicated that the remaining iron is in the crystalline structure of kaolinite. This result was confirmed by EPR and ES.

pH and Eh control during chemical bleaching is of fundamental importance to guarantee iron removal and inhibit any possibility of elementary sulfur precipitation, which can interfere in kaolin's brightness.

Kaolin from the Borborema–Seridó region has some characteristics that indicate the feasibility of its use mainly as a filler in the paper industry, as well as in paint, pottery, rubber and other industries. It is worth highlighting that in order to reach the specification as a coating agent in the paper industry (70–90% < 2 μm) it is necessary to submit it to a subsequent centrifugation step.

Acknowledgements

References

Brindley et al., 1986 G.W. Brindley, C.C. Kao, J.L. Harrison, M. Lipsicas and R. Raythatha, Relation between structural disorder and other characteristics of kaolinites and dickites, *Clays and Clay Minerals* **34** (1986), pp. 239–249. View Record in Scopus | Cited By in Scopus (80)

Ciullo, 2004 P.A. Ciullo, Kaolin Clay: Functional Optical Additives (2004) www.pcimag.com/CDA/articleinformation/features/BNP_Features_Item/0,1846,105008,00.html.

Clozel et al., 1994 B. Clozel, T. Allard and J.P. Muller, Nature and stability of radiation induced defects in natural kaolinites: new results and a reappraisal of published works, *Clays and Clay Minerals* **42** (6) (1994), pp. 657–666. View Record in Scopus | Cited By in Scopus (35)

Conceição et al., 2005 S. Conceição, N.F. Santos, J. Velho and J.M.F. Ferreira, Properties of paper coated with kaolin: the influence on the rheological modifier, *Applied Clay Science* **30** (2005), pp. 165–173. **Article** | PDF (171 K) | View Record in Scopus | Cited By in Scopus (1)

Domenico, 2000 J.E.J. Domenico, The role of physical processing enhancing the quality of industrial mineral, *14th Industrial Minerals International Congress, Denver, Colorado* (2000).

Luz and Chaves, 2000 A.B. Luz and A.P. Chaves, *Tecnologia do Caulim: ênfase na indústria de papel*, *Rochas e Minerais Industriais* **vol. 01**, Centro de Tecnologia Mineral (2000).

Luz et al., 2005 A.B. Luz, A.R. Campos, E.A. Carvalho and L.C. Bertolino, Caulim: Usos e Especificações. In: A.B. Luz and F.F. Lins, Editors, *Rochas e Minerais Industriais* (1st ed.), Centro de Tecnologia Mineral, Rio de Janeiro, Brasil (2005) cap. 11.

Marel and Beutelspacher, 1976 H.W. Marel and H. Beutelspacher, Atlas of Infrared Spectroscopy of Clay Minerals and Their Admixtures (1st ed.), Elsevier Scientific Publishing Company, Amsterdam (1976).

Murray and Kogel, 2005 H.H. Murray and J.E. Kogel, Engineered clay products for the paper industry, *Applied Clay Science* **28** (2005), pp. 199–206. View Record in Scopus | Cited By in Scopus (14)

Prasad et al., 1991 M.S. Prasad, K.J. Reid and H.H. Murray, Kaolin: processing, properties and application, *Applied Clay Science* **06** (1991), pp. 87–119. Abstract | View Record in Scopus | Cited By in Scopus (18)

Silva and Dantas, 1997 M.R.R. Silva and J.R.A. Dantas In: DNPM/CPRM, Editor, *Província pegmatítica da Borborema–Seridó, Paraíba e Rio Grande do Norte* (1st ed),

Principais Depósitos Minerais do Brasil **vol. 4b**, Departamento Nacional de Produção Mineral, Brasília, Brasil (1997).

Wilson et al., 1998 I.R. Wilson, H.S. Santos and P.S. Santos, Caulins brasileiros: alguns aspectos da geologia e da mineralogia, *Cerâmica* **44** (287–288) (1998), pp. 118–129.

Corresponding author. Tel.: +55 21 38657359, +55 21 38657203, +55 21 22909196.